

Linear and Time-Dependent Behavior of the Gyrotron Backward-Wave Oscillator

S. H. Chen,¹ T. H. Chang,² K. F. Pao,³ C. T. Fan,³ and K. R. Chu³

¹National Center for High-Performance Computing, Hsinchu, Taiwan

²National Center for Theoretical Sciences, Hsinchu, Taiwan

³Department of Physics, National Tsing Hua University, Hsinchu, Taiwan

(Received 16 August 2002; published 10 December 2002)

Formation of axial modes in the gyrotron backward-wave oscillator is examined in the perspective of optimum conditions for beam-wave interactions. Distinctive linear properties are revealed and interpreted physically. Nonlinear implications of these properties (specifically, the role of high-order axial modes) are investigated with time-dependent simulations. Nonstationary oscillations exhibit self-modulation behavior while displaying no evidence of axial mode competition. Reasons for the erratic frequency tuning are investigated and stable tuning regimes are identified as a remedy.

DOI: 10.1103/PhysRevLett.89.268303

PACS numbers: 84.40.Ik, 84.40.Fe

The gyrotron backward-wave oscillator (gyro-BWO) is a frequency tunable version of the gyrotron. Oscillations build up via the electron cyclotron maser interaction in an *internal* feedback loop composed of the forward moving electron beam and a backward propagating wave. Theoretical studies of the gyro-BWO first appeared in the mid-1960s in the Soviet literature (reviewed in [1]). Linear theory [2–4] forms the first theoretical basis by predicting the start-oscillation conditions. Orbit tracing techniques [1,5–10] and particle simulations [11] are then employed to investigate the nonlinear behavior.

Since no cold resonant mode exists in the gyro-BWO interaction structure (essentially a waveguide), the existence of oscillating modes must then depend entirely on the beam-wave interaction. The physics underpinning is thus expected to be fundamentally different from oscillations in a resonant structure, for which each hot mode has a corresponding cold mode. For example, it has recently been shown that the axial field profile contracts nonlinearly, which results in stable operation at currents orders-of-magnitude higher than the start-oscillation current [9,10]. Further studies reveal that stationary and nonstationary states alternately appear as the beam current rises [12,13]. Excitation of high-order axial modes (HOAMs) has been suggested as a possible cause of the nonstationary behavior involving tapered interaction structures [12,13]. However, unbalanced beam energy deposition is also known to result in self-modulation of a single mode [10,14–16].

For a resolution of this and other fundamental issues, an indepth knowledge of the axial modes is clearly important. The current work begins with a physics characterization of the axial modes in the linear stage. This is followed by time-dependent simulations of the gyro-BWO as a nonlinear system. Linear and nonlinear dynamics reveal the nature of the nonstationary behavior as well as properties specific to the gyro-BWO, such as the accessibility of HOAMs and broadband frequency tunability with respect to the applied magnetic field.

Model, assumptions, and numerical methods.—For purposes of brevity and clarity of exposition, we model the basic gyro-BWO circuit (Fig. 1) with a uniform waveguide 0.2654 cm in radius (r_w) and assume a cold electron beam in the presence of a uniform magnetic field (B_0). The electron voltage (V_b) is fixed at 95 kV with a perpendicular-to-parallel velocity ratio (α) of 1.1 and guiding centers positioned at $r_c = 0.35r_w$. With $B_0 > 14.02$ kG, the electron beam interacts with the backward TE_{11} wave at the fundamental cyclotron harmonic. A steady-state code [17] is employed in conjunction with a time-dependent code, both assuming the transverse field structure to be that of the cold TE_{11} mode. The steady-state code imposes single-frequency oscillations, while the time-dependent code allows the excitation of multiple axial modes. Both the linear and nonlinear solutions are obtained under the outgoing-wave boundary conditions, rather than the commonly employed condition of infinite gain [1–6,18,19].

Linear behavior and physical interpretations.—Fig. 2 displays typical axial dependence of the field amplitude (unbroken curves), phase angle (dots), and beam energy deposition rate (dashed curves) for the first four axial modes at their respective start-oscillation current (I_{st}). The rf fields (Fig. 2), while bearing resemblance to the resonator modes, assume entirely different characters. First, these fields represent essentially backward traveling waves, rather than standing waves, as indicated by their monotonically decreasing phase angles (except for a short section near the downstream end). Second, multiple

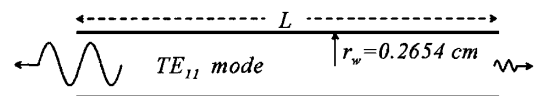


FIG. 1. Configuration and dimensions of the gyro-BWO under study. Beam parameters for all figures are fixed at $V_b = 95$ kV, $\alpha = 1.1$, and $r_c = 0.35r_w$. The beam current I_b , interaction length L , and applied magnetic field B_0 are varied.

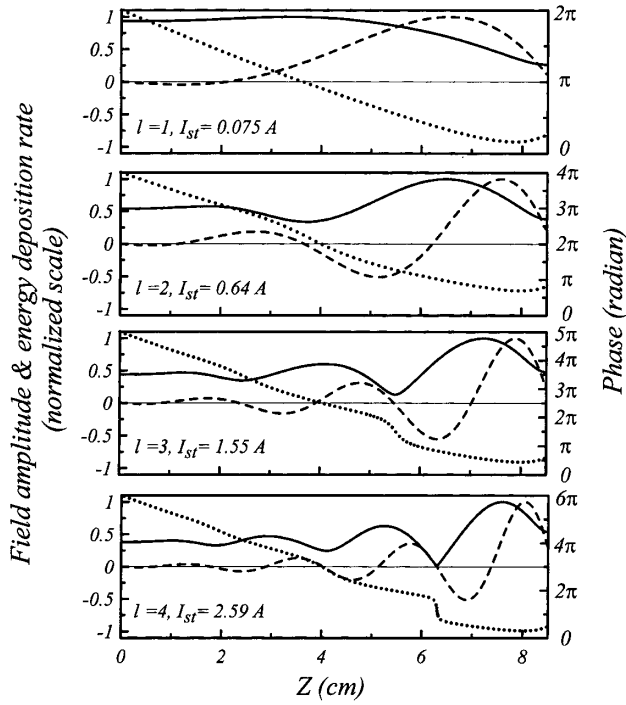


FIG. 2. Axial dependence of the field amplitude (unbroken curves), phase angle (dotted curves), and beam energy deposition rate (dashed curves) for the first four axial modes at their respective I_{st} (see Fig. 4). $L = 8.5$ cm and $B_0 = 14.5$ kG.

amplitude troughs of the HOAMs ($l > 1$) principally result from energy reabsorption by the beam in regions of negative energy deposition (Fig. 2), rather than the destructive interference between forward and backward traveling waves. Thus, as the wave propagates backwards, an amplitude trough forms following each region of negative energy deposition. Linearly, the number of regions of positive energy deposition determines the order of the axial mode. Physical interpretations as well as further insight are provided by examination of the electron transit angle (Θ) defined as

$$\Theta = (\omega - k_z v_{z0} - \Omega_c)\tau, \quad (1)$$

where ω and k_z are, respectively, the wave frequency and cold circuit propagation constant ($k_z < 0$ for backward waves), Ω_c is the relativistic electron cyclotron frequency, and $\tau = L/v_{z0}$ is the electron transit time at their initial velocity v_{z0} . With $k_z < 0$, the transit angle provides a measure of the total phase variation of the backward wave as experienced by the electrons in traversing the interaction space. For the HOAMs, the rate of beam energy deposition varies periodically between positive and negative maxima along the z axis (Fig. 2); the higher the wave frequency ω , the shorter the spatial period. This results in periodic variation of the *integrated* beam energy deposition with respect to ω , and consequently Θ . Thus, the total deposited power maximizes at a discrete set of optimum values of Θ . At each optimum Θ , the output wave power and deposited beam power reach a

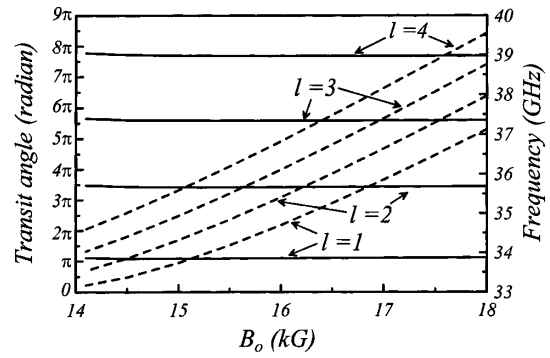


FIG. 3. Transit angle (unbroken curves) and start-oscillation frequency (dashed curves) versus B_0 for the first four axial modes. $L = 8.5$ cm.

balance at a beam current minimum, which yields the start-oscillation current of an axial mode.

It is interesting to note from Fig. 3 that each axial mode in its linear stage is characterized by the *constancy* of the electron transit angle regardless of the magnetic field. Physically, this is because the nonresonant interaction structure allows the start-oscillation frequency to vary in concert with the magnetic field (Fig. 3) such that Θ remains at the optimum value for maximum interaction strength. Consistent with the interaction picture (Fig. 2), optimum transit angles of the axial modes are separated by $\sim 2\pi$ from mode to mode (Fig. 3). In contrast, optimum transit angles for all orders of axial modes of the gyromonotron fall in the neighborhood of $\sim \pi$ [20].

Implications of linear theory.—Larger transit angles for the HOAMs result in more regions of beam energy reabsorption (Fig. 2), hence reduced interaction strength. As a result of this and the higher diffractive power loss of the HOAMs, the start-oscillation current increases with l (Fig. 4), given the same interaction length for all axial modes. The fundamental axial mode ($l = 1$) will always appear first as the beam power rises from below the oscillation threshold. This suggests that excitation of the HOAMs is inherently a multimode effect. Dominance of a HOAM, if possible, will then be the consequence of mode competition.

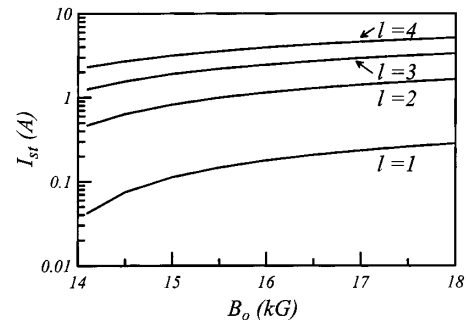


FIG. 4. Start-oscillation current versus B_0 for the first four axial modes. $L = 8.5$ cm.

Furthermore, the large separation (by a factor of ~ 8) [21] between I_{st} of the fundamental mode ($l = 1$) and the first HOAM ($l = 2$) suggests a substantial buildup of the fundamental mode as the beam current continues to rise to the threshold of the first HOAM. Since the formation of axial modes depends entirely on the beam-wave interaction, questions arise as to the accessibility as well as identities of the HOAMs defined on the basis of the single-mode theory, given the presence of a large-amplitude fundamental mode. These issues will be addressed below with time-dependent simulations.

Time-dependent behavior.—The time-dependent code has been employed to characterize the dynamical behavior in the parameter space of the beam current (I_b) and interaction length (L) (Fig. 5). Superposed on the stability map are I_{st} of the first four axial modes (dashed curves) obtained with the single-mode, steady-state code. The appearance of multiple zones of nonstationary states in the $I_b - L$ space has been previously reported [12,13] for the case of tapered interaction structures. Reasons for such behavior are still unclear. No attempt at a full interpretation will be made here. Instead, in the interest of its avoidance, we shall focus our attention to the onset stage of the nonstationary state.

Figure 5 shows excellent agreement between I_{st} of the fundamental axial mode obtained by both codes. However, there is no correlation between the onset current of the nonstationary state (obtained by the time-dependent code) and I_{st} of HOAMs (obtained by the single-mode code). For example, oscillations can either remain stable at beam currents far above I_{st} of the $l = 4$ mode (for $L < 8$ cm) or turn nonstationary at currents well below I_{st} of the $l = 2$ mode (for $L > 11$ cm). This suggests a cause for the nonstationary behavior other than axial mode competition, as well as validates our earlier contention concerning the inaccessibility of HOAMs.

It is also worth noting that the threshold currents for the nonstationary states shown in Fig. 5 range from 4 to more than 100 times I_{st} . Except for the case of a long interaction length, this is in sharp contrast with the nonstationary threshold current of the conventional BWO

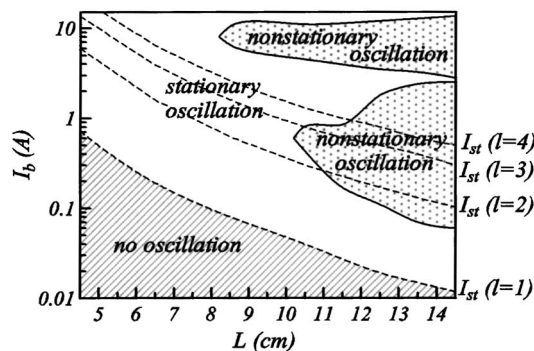


FIG. 5. Stability map in the $I_b - L$ space. $B_0 = 14.5$ kG.

which in some studies was reported to be 2.5–3.5 times I_{st} , in theory [22,23] and in experiment [24]. Nonlinear field contraction of the gyro-BWO mode [9], which delays the onset of the nonstationary state, is a likely cause for the difference.

Figure 6 displays the (calculated) output spectra at currents slightly above the onset of the nonstationary state for $L = 8.5$ and 12 cm. The spectra, composed of equally spaced sidebands about a main peak, exhibit self-modulation behavior of the fundamental axial mode. In such a state, the uneven spatial distribution of the beam deposited energy causes the field energy to bounce back and forth within the feedback loop and, hence, modulates the oscillation amplitude and generates the sidebands. The frequency difference between the main oscillation and the sidebands is greater for $L = 8.5$ cm than for $L = 12$ cm, consistent with the higher oscillation frequency (hence faster group velocity) and shorter bounce distance in the former case.

Frequency tuning.—In most gyro-BWO experiments, erratic power output was observed during frequency tuning (discussed in [9]). Figures 5 and 6 point to self-modulation as a likely cause and it can be remedied with a shorter interaction length, as is verified in the stability map in the $I_b - B_0$ space (Fig. 7). Figure 7(a) shows a broad, stable tuning range over both I_b and B_0 for $L = 4.5$ cm. Stability then deteriorates with increased L [Fig. 7(b)]. For $L = 12$ cm, only isolated regions are stable except for very low beam currents [Fig. 7(c)].

In summary, linear behavior of the gyro-BWO is elucidated in the perspective of optimum beam-wave interactions. Knowledge of the formation processes of individual axial modes provides the requisite groundwork for an examination of the nonstationary behavior, as well

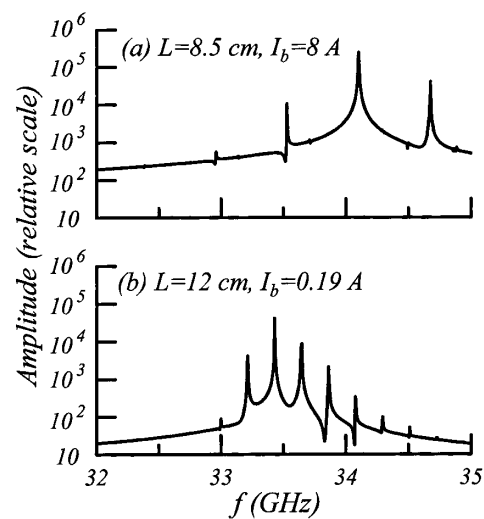


FIG. 6. Output spectra at $B_0 = 14.5$ kG and I_b slightly above the threshold current of the nonstationary state for (a) $L = 8.5$ cm and (b) $L = 12$ cm.

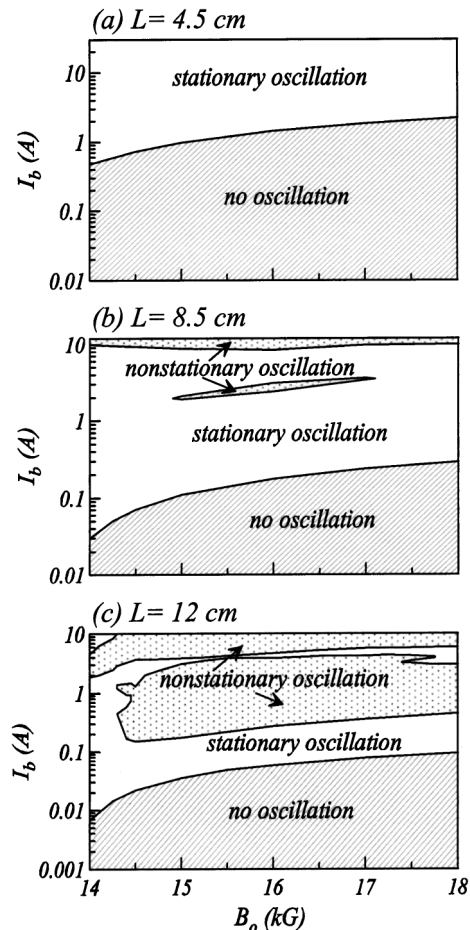


FIG. 7. Stability map in the $I_b - B_0$ space. (a) $L = 4.5$ cm, (b) $L = 8.5$ cm, and (c) $L = 12$ cm.

as the accessibility and identity of HOAMs. Non-stationary oscillations at the onset stage exhibit self-modulation behavior, which might have caused the erratic frequency tuning commonly observed in experiments. Regimes of stable magnetic field tuning are identified as a result.

This work was sponsored by the National Science Council, Taiwan. The authors are grateful to Dr. T. M. Antonsen, Dr. N. C. Luhmann, Jr., Dr. G. S. Nusinovich, and Dr. A. N. Vlasov for helpful discussions.

[1] G. S. Nusinovich and O. Dumbrajs, *IEEE Trans. Plasma Sci.* **24**, 620 (1996).

- [2] J. M. Wachtel and E. J. Wachtel, *Appl. Phys. Lett.* **37**, 1059 (1980).
- [3] S. Y. Park, V. L. Granatstein, and R. K. Parker, *Int. J. Electron.* **57**, 1109 (1984).
- [4] C. S. Kou, *Phys. Plasmas* **1**, 3093 (1994).
- [5] V. K. Yulpatov, *Radiophys. Quantum Electron.* **10**, 471 (1967).
- [6] A. K. Ganguly and S. Ahn, *Appl. Phys. Lett.* **54**, 514 (1989).
- [7] M. Caplan, in *Conference Digest: 12th International Conference on Infrared Millimeter Waves* (IEEE, Piscataway, NJ, 1987), p. 276.
- [8] C. S. Kou, C. H. Chen, and T. J. Wu, *Phys. Rev. E* **57**, 7162 (1998).
- [9] S. H. Chen, K. R. Chu, and T. H. Chang, *Phys. Rev. Lett.* **85**, 2633 (2000).
- [10] T. H. Chang, S. H. Chen, L. R. Barnett, and K. R. Chu, *Phys. Rev. Lett.* **87**, 064802 (2001).
- [11] A. T. Lin, *Phys. Rev. A* **46**, 4516 (1992).
- [12] G. S. Nusinovich, A. N. Vlasov, and T. M. Antonsen, Jr., *Phys. Rev. Lett.* **87**, 218301 (2001).
- [13] A. Grudiev and K. Schunemann, *IEEE Trans. Plasma Sci.* (to be published).
- [14] N. S. Ginzburg, G. S. Nusinovich, and N. A. Zavol'sky, *Int. J. Electron.* **61**, 881 (1986).
- [15] A. T. Lin, Z. H. Yang, and K. R. Chu, *IEEE Trans. Plasma Sci.* **16**, 129 (1988).
- [16] A. Y. Dmitriev, D. I. Trubetskov, and A. P. Chetverikov, *Izv. Vyssh. Uchebn. Zaved. Radiofiz.* **34**, 595 (1991) [*Radiophys. Quantum Electron.* **34**, 502 (1991)].
- [17] K. R. Chu, H. Y. Chen, C. L. Hung, T. H. Chang, L. R. Barnett, S. H. Chen, T. T. Yang, and D. Dialetis, *IEEE Trans. Plasma Sci.* **27**, 391 (1999).
- [18] H. R. Johnson, *Proc. IRE* **43**, 684 (1955).
- [19] M. Chorodow and C. Susskind, *Fundamentals of Microwave Electronics* (McGraw-Hill, New York, 1964), Chap. 7.
- [20] See, for example, V. A. Flyagin and G. S. Nusinovich, *Proc. IEEE* **76**, 644 (1988).
- [21] Perhaps for the same reason, the separation in the conventional BWO is even greater (by a factor of ~ 81). See Refs. [18,19].
- [22] N. S. Ginzburg, S. P. Kuznetsov, and T. N. Fedoseeva, *Izv. Vyssh. Uchebn. Zaved. Radiofiz.* **21**, 1037 (1978) [*Radiophys. Quantum Electron.* **21**, 728 (1978)].
- [23] B. Levush, T. M. Antonsen, A. Bromborsky, W. R. Lou, and Y. Carmel, *IEEE Trans. Plasma Sci.* **20**, 263 (1992).
- [24] B. P. Bezruchko and S. P. Kuznetsov, *Izv. Vyssh. Uchebn. Zaved. Radiofiz.* **21**, 1053 (1978) [*Radiophys. Quantum Electron.* **21**, 739 (1978)].